Airstream Boundaries in Numerical Weather Simulations

ROBERT A. COHEN* AND CARL W. KREITZBERG

Department of Physics and Atmospheric Science, Drexel University, Philadelphia, Pennsylvania

(Manuscript received 9 June 1995, in final form 16 May 1996)

ABSTRACT

Distinct airstreams, separated by sharp boundaries, are present in numerical weather simulations and can be used to identify characteristic structures in baroclinic storms. To allow objective comparisons between different analyses, a rigorous treatment of airstream boundaries is performed based upon a numerical procedure in which the uncertainty of individual trajectory paths is related to the strength of an airstream boundary, as defined and quantified herein. The properties of the procedure are then investigated via application to a numerical simulation of the ERICA IOP 4 storm. The work not only provides the necessary framework within which future analyses of airstreams can be interpreted but also provides insights into quantitative properties of atmospheric flows.

1. Overview and purpose

One way of describing the development of an extratropical cyclone is in terms of its frontal evolution. Other structures, which may or may not be related to the fronts, are also present, however, and thus can also be used in this description. In this respect, airstreams and their boundaries have been popular (see section 2). Unfortunately, identifying the distinct airstreams is often a time consuming and subjective process; it is time consuming in the sense that one must sort through an ensemble of trajectories to delineate the source regions and subjective in the sense that distinguishing between airstreams has never been quantified. To address these problems, a technique is introduced that utilizes the computer's ability to analyze trajectories en masse.

The technique presented here is just one way of using the computer to analyze an ensemble of trajectories and thus avoid the process of plotting and sorting through each trajectory individually. Information regarding the general characteristics of the flow can be obtained by color coding the source position (Pierrehumbert and Yang 1993; Sutton 1994) or using isopleths of displacement (Schär and Wernli 1993). The procedure outlined here, however, quantifies the analysis and, as such, provides a base upon which airstream boundaries can be numerically described and characterized. These characteristics, as diagnosed from numerical simulations, are presented along with some potential applications of the results. The sensitivity of the diagnostic technique to the calculation procedure is also addressed (see section 6).

Before proceeding with the quantitative analysis of airstream boundaries, the following items are carried out (see section 2).

1) *Airstream* is defined and contrasted with related terms (e.g., *air mass*).
2) *Airstream boundary* is defined and contrasted with related terms (e.g., *front*).
3) The strength of an airstream boundary is quantitatively defined.

The strength of an airstream boundary is then used to define and identify a vertical to horizontal scale and a graphing criterion, both of which are necessary before airstream boundaries can be identified (see section 4). By clearly defining the parameters, subjectivity is minimized, allowing criticisms of the resulting analysis to focus on the interpretations and conclusions based upon the analysis.

2. Definitions

a. Airstreams

As far as the authors know, a formal distinction between *air currents*, *airstreams*, and *air masses* has never been made. It is known, however, that up until the early part of this century, it was common to describe extratropical cyclone structure in terms of distinct air currents (see, e.g., the upper and lower currents of Ley 1877; see also Kutzbach 1979). During this time, the term

*Current affiliation: Department of Physics, East Stroudsburg University, East Stroudsburg, Pennsylvania.

Corresponding author address: Dr. Robert A. Cohen, Dept. of Physics, East Stroudsburg University, East Stroudsburg, PA 18301. E-mail: bbq@esu.edu

appears to have been used in place of the more ambiguous term *wind* (as in the *trade winds* of Halley 1686) as an atmospheric analog to the oceanic current. Following the lead of Sir Napier Shaw (Shaw and Lempfert 1905), who did work on cyclone structure similar to that presented here but with techniques that are now obsolete, an *air current* is defined herein as a region of air in which the spatial history of each portion is similar.

With the development of the polar front theory (Bjerknes and Solberg 1922) and its emphasis on temperature contrasts, the popularity of the *air currents* waned in favor of the *air masses,* that is, a region of air characterized by similar thermodynamic properties (Huschke 1959). Still, when straying from the polar front model, meteorologists have tended to use terms similar to the *air current.* Thompson (1951), for example, in his analysis of upper-air charts, identified boundaries between *airflows* of different histories. When satellite pictures became available in the 1960s, the focus upon air currents again became popular (see, e.g., the *conveyor belts* of Browning 1971) in part because the boundaries of cloud and weather patterns could be related to *airstream* boundaries (Carlson 1980). Currently, *airstream* appears to the preferred term (see, e.g., Schultz and Mass 1993) and so is used herein in preference to the other terms. However, the various terms are synonymous. Indeed, *Webster's New Collegiate Dictionary* (Woolf 1979) defines *airstream* as a current of air, and Shaw tended to use the terms *trade-wind, air-current,* and *stream of air* interchangably (see, e.g., Shaw 1928, p. 249).

b. Airstream boundaries

Based upon the definition of *airstream* presented above, it is straightforward to define an airstream boundary as a surface separating two relatively distinct airstreams. Admittedly, ''relatively distinct'' is inexact, and one purpose of this paper is to provide a measure of airstream differences so that airstream boundaries can be identified in a straightforward manner (see section 4).

Before proceeding further, however, the difference between an *airstream boundary* and an *airmass boundary* is addressed. While the difference between an *airstream* and an *air mass* is relatively clear, in practice the difference between an *airstream boundary* and an *airmass boundary* is not clear. The ambiguity can be traced to the development of the frontal terminology. In the late nineteenth century, the kinematic way of describing cyclone development (i.e., one in which the interplay of currents produced the cyclone) gave way to a more thermodynamic approach (i.e., one in which the coexistence of different air masses produced the cyclone). Yet, even as the focus changed from air currents to air masses, it remained popular to describe the cyclone structure in terms of the air currents.

For example, what we now call the cold front was typically associated with a northerly current invading, and forcing its way under, a southerly current (see, e.g., Lempfert and Corless 1910). Even Bjerknes and Solberg (1922), who argued that the energy for the cyclone lay in air masses of contrasting temperatures, clearly relate the *polar front* to the boundary between the polar and tropical air currents. In keeping with this viewpoint, they saw the polar front as existing even when the temperature contrast became indistinct or vanished, suggesting that trajectories could be used to distinguish between the two airmass origins and thus identify the front.

In this sense, there is no difference between an airstream boundary and a front. Eventually, however, the *front* became synonymous with an *airmass boundary* and, as such, became an entity distinct from an *airstream boundary.* Current practice now associates a front with gradients in an instantaneous field (i.e., density), while the airstream boundary, as defined above, is associated with gradients in a time-integrated field (i.e., spatial history). It is recognized that the two can coincide (see, e.g., the analysis of the occluded front by Schultz and Mass 1993) but such coincidence is not to be assumed.

c. Strength of airstream boundaries

Two nearby parcels will have similar histories if both parcels are within the same airstream. Conversely, two nearby parcels will have dissimilar histories if the parcels straddle an airstream boundary. In other words, the history of an air parcel near an airstream boundary is more highly dependent upon its location than the history of an air parcel far from an airstream boundary. The strength of an airstream boundary, then, is related to the dependence of a coincident parcel's history upon its location.

To quantify this dependence, the authors borrow a procedure used in studies of chaotic mixing (see, e.g., Pierrehumbert and Yang 1993). In such studies, the Lyapunov exponent is used as a measure of the maximum uncertainty of a particle's future position as a result of the uncertainty in its initial position. Here, our interest is in the maximum uncertainty of a particle's past position.

To illustrate, consider a group of parcels arranged in a circular ring of diameter $r(0)$. With time, the ring is expected to evolve into an ellipse. For chaotic flow, the major axis, r, grows exponentially with time t as follows (see section 4 for the physical mechanism responsible):

$$r(t) = r(0)\exp(\lambda t) \text{ and } \qquad t > 0.$$

The coefficient λ provides the elongation rate (known as the Lyapunov exponent in phase space). The larger the elongation rate, the more highly dependent a parcel's future path is upon its position at time zero.

For our purposes, it is proposed to do the same for the ring history. At some earlier time t, the ring is an ellipse. Its major axis r contracts over time such that, at earlier times,

$$r(t) = r(0)\exp(-Ct) \text{ and } \qquad t < 0, \qquad (1)$$

where C is identical to λ except that the ellipse is evolving toward, rather than from, the state of the ring. Whereas λ represents the future elongation rate of the major axis, C represents its prior contraction rate. The larger the contraction rate, the more highly dependent a parcel's *history* is upon its position at time zero.

Thus, C is a measure of the strength of an airstream boundary. By solving for C in (1), the contraction rate is obtained as follows:

$$C = -\frac{1}{t}\ln\left[\frac{r(t)}{r(0)}\right]; \qquad t < 0. \qquad (2)$$

Although chaotic flow implies that trajectories will diverge exponentially (going backward in time), the contraction rate need not be constant with time for the purposes of this paper (see section 4d). The logarithmic expression is a natural consequence of what the contraction rate represents—that is, the average reduction in separation of two parcels relative to each other. To see why this is, consider the instantaneous reduction in separation of two parcels relative to each other, $c = -v(t)/r(t)$. Since $v = dr/dt$,

$$c = -\frac{dr(t)}{r(t)dt} = -\frac{d\ \ln r(t)}{dt},$$

and the average rate can be written as

$$C = -\frac{1}{t}\int_0^t \frac{d\ \ln r(t)}{dt}dt,$$

which gives the same form as (2). Thus, the contraction rate represents a Lagrangian, time-averaged contraction of the ellipse.

3. Calculation of contraction rates

Ideally, the contraction rate at a particular grid point would be determined via an infinite number of parcels arranged on the surface of a sphere of infinitessimal size centered at the grid point. Consequently, there would be an infinite number of parcel pairs that straddle the center point and lie on opposite sides of the sphere. The contraction rate would then be calculated for each parcel pair, and the greatest would be used as the contraction rate valid at the center.

In practice, a grid of finite spacing is used. The contraction rate at a particular grid point is determined via the parcels at the 26 surrounding grid points, that is, 8 on the same horizontal plane and 9 each on the planes immediately above and below (see Fig. 1). These 26 parcels form 13 parcel pairs. The contraction rate is determined for each parcel pair, and the greatest is used as the contraction rate valid at the center grid point.

For this study, the contraction rate is determined in this way for a 99 × 59 × 49 grid (0.3° spacing in the horizontal and 0.2-km spacing in the vertical, hereafter the trajectory grid). The vertical coordinate is in sigma kilometers such that a zero height corresponds to the surface and heights above 5.5 km correspond to the geopotential height. The numerical simulations are carried out by the Limited Area and Mesoscale Prediction System,[1] a hydrostatic, full physics numerical model with a horizontal grid spacing of about 70 km and 34 vertical levels of 0.5-km spacing above the boundary layer. To better define the features, the trajectory grid is finer than the model simulation grid. The horizontal domains of the model and trajectory grids are indicated in Fig. 2.

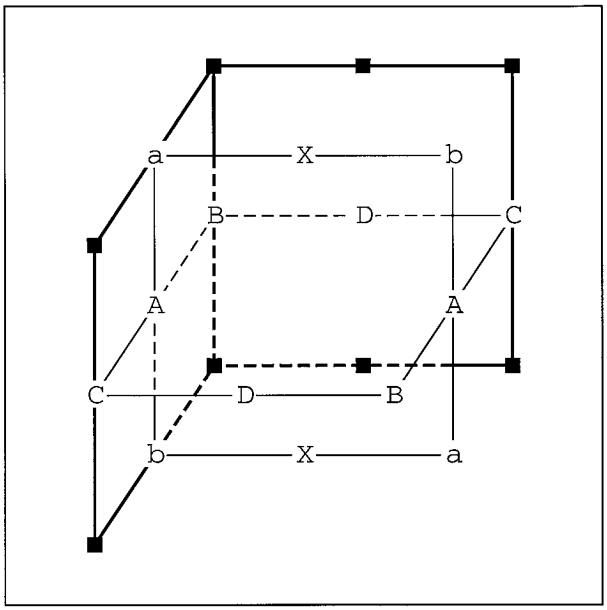

FIG. 1. The configuration of the 26 points surrounding a grid point (only 22 are shown). The 26 points can be grouped into 13 pairs as follows: 4 pairs are in the horizontal plane (*AA*, *BB*, *CC*, and *DD*), 1 pair is along the vertical axis (*XX*), and the remaining pairs are separated both in the vertical and horizontal (e.g., *aa* and *bb*).

Two simulations are made of the IOP (intensive observation period) 4 storm studied as part of the Experiment on Rapidly Intensifying Cyclones over the Atlantic (ERICA; Hadlock and Kreitzberg 1988). The storm developed off the Atlantic coast of the United States (near 35°N, 75°W) around 0000 UTC 4 January 1989 and deepened rapidly as it traveled eastward along the northern border of the Gulf Stream (see Fig. 3). Most of the drop in central sea level pressure occurred by 1800 UTC 4 January 1989 (see Fig. 4). For a detailed discussion of the observed storm see Chang et al.

[1] Available from the Numerical Model Development Facility, Dept. of Physics and Atmospheric Science, Drexel University, Philadelphia, PA 19104. Also available in tar format via the World Wide Web at ftp://nimbus.physics.drexel.edu/lamps90.html. See the URL for dynamic model documentation.

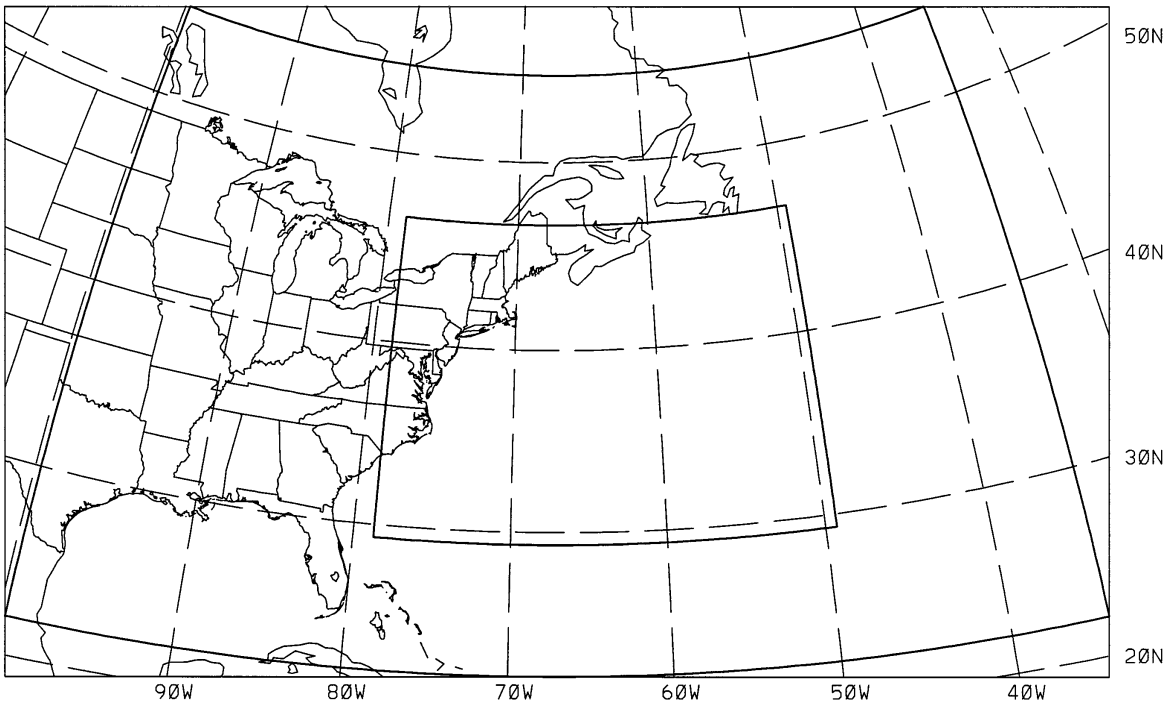

FIG. 2. Horizontal limits of the model (outer box) and trajectory (inner box) grids.

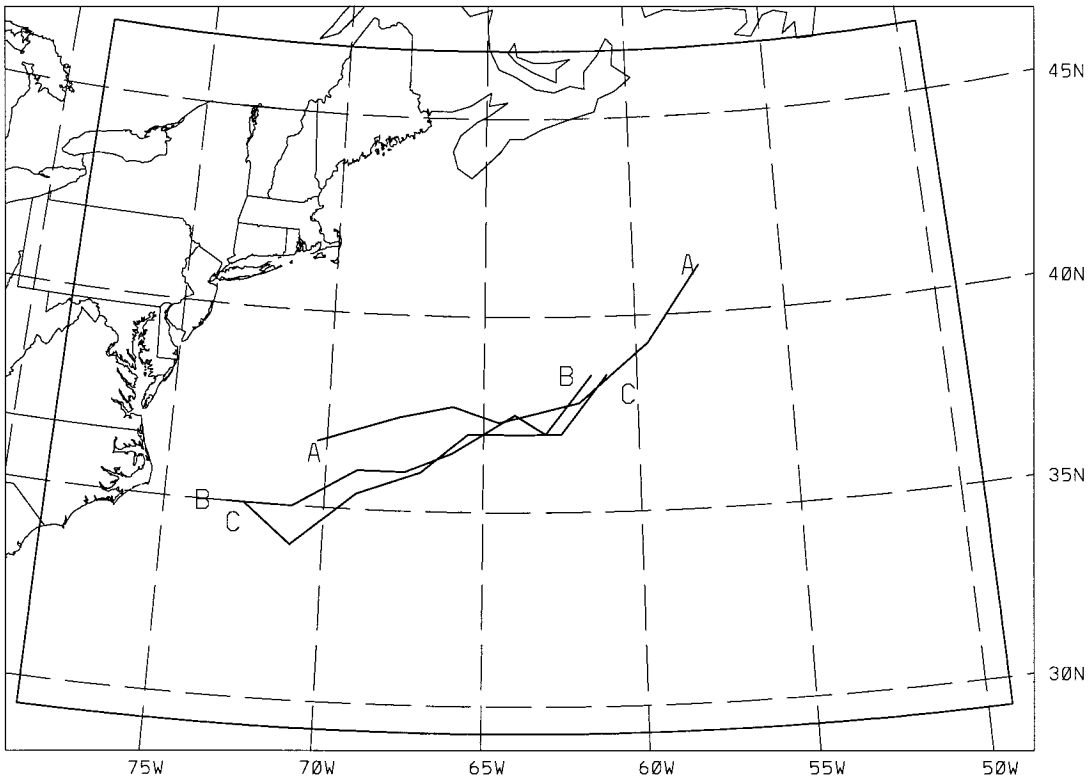

FIG. 3. Track of sea level pressure minimum for the observed and simulated ERICA IOP 4 storms, from 0300 UTC 4 January 1989 to 0000 UTC 5 January 1989 (A, observed; B, simulation initialized at 1200 UTC 3 January 1989; C, simulation initialized at 0000 UTC 4 January 1989). The observed location is taken from Hartnett et al. (1989). Box corresponds to the horizontal limit of the trajectory grid.

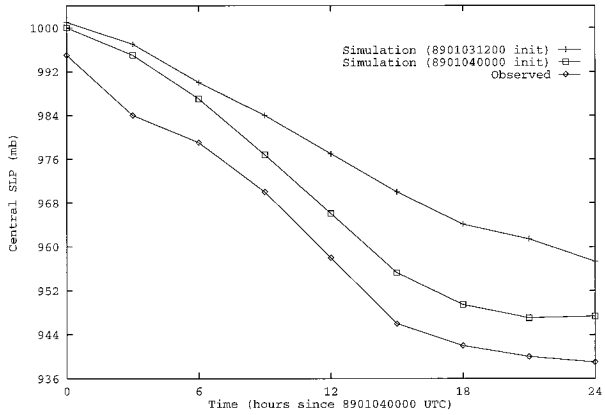

FIG. 4. Evolution of the sea level pressure minimum for the observed and simulated ERICA IOP 4 storms (diamonds, observed; crosses, simulation initialized at 1200 UTC 3 January 1989; boxes, simulation initialized at 0000 UTC 4 January 1989). The observed central pressure is taken from Hartnett et al. (1989).

(1993), Neiman and Shapiro (1993), Neiman et al. (1993), and Wakimoto et al. (1992).

The two simulations cover the same domain but are initialized at different times. One is initialized at 1200 UTC 3 January 1989 and run for 36 h, with wind data saved every hour. The second simulation is initialized at 0000 UTC 4 January 1989 and run for 24 h, with wind data saved every 15 min. The first simulation is used in the next section to investigate the properties of the contraction rate. The longer simulation time is needed to calculate contraction rates both early and late in the life of the storm. The second simulation is used in section 6 to investigate the sensitivity of the diagnostic technique to the calculation procedure, which requires an increased frequency of wind data. The second simulation is also used in section 7, where the later initialization time provides a more realistic simulation, allowing comparisons to be made between the simulated airstream boundaries and analyzed fronts.

Qualitatively, the ability of the model to reconstruct the general characteristics of the storm is quite good in that the cloud signatures produced in the simulations are similar to the satellite pictures (not shown). Quantitatively, the placement and development of the circulation center lagged somewhat to the south and west of that observed (see Fig. 3) and the amount of deepening was underpredicted, as measured by the central sea level pressure (see Fig. 4). For the purposes of this paper, however, getting the best possible simulation is not critical. It is the general character of extratropical storms, not the specific structure of a particular event, that is being analyzed, and it is believed that the general character has, indeed, been adequately simulated.

During each simulation, the three-dimensional wind values for the entire model domain are saved every t_m (hereafter the wind data step). A wind field every t_i (hereafter the integration step) is determined via linear interpolation in time from the saved wind data. At each grid point of the trajectory grid, a trajectory is determined via the following procedure.

1) The wind data at the grid point are determined via linear interpolation (in space) from the model grid.
2) This wind data are recalculated according to the following procedure n times (hereafter the number of wind correction steps).
   (a) Using the interpolated wind field, an estimate of the air parcel displacement during the previous t_i is calculated.
   (b) Using the estimate of the air parcel displacement, the position of the air parcel t_i earlier is determined.
   (c) The wind field at this new position and time is determined via linear interpolation (in space).
   (d) An average wind is calculated using the winds from the old and new positions.
3) Using the calculated average wind speed, an estimate of the air parcel displacement during the previous t_i is calculated.
4) At the new position, the wind is determined via linear interpolation (in space).
5) Steps 2 and 3 are repeated; that is, the wind is corrected n times and the air parcel displacement is estimated.
6) Steps 4 and 5 are repeated until t is reached (hereafter the trajectory lifetime).

For the next section, $|t|$ is 12 h, t_m is 60 min, t_i is 15 min, and n is 2. The latter three values represent a balance between space and sensitivity considerations (see section 6). Twelve hours is used because the characteristic timescale for rapid development in this storm (as measured by the sea level pressure minimum) is about 12 h and similar timescales have been noticed in other rapidly intensifying storms (see Uccellini 1990). Unless noted otherwise, the discussion in the next section is not expected to be sensitive to these parameters.

4. Discussion

a. General properties

Although no assumption is made regarding the constancy of the contraction rate, it is recognized that, in general, C will tend to have a positive value. That is, given a long enough history, two nearby parcels are expected to have originated from separate locations (and will travel to separate locations in the future).

To see why this is, consider that the instantanous flow of one parcel relative to another will have two components, that is, along and normal to the line separating the two parcels (see Fig. 5). The flow along the line is convergent or divergent. The flow normal to the line is shearing.

For the immediate past and future, the convergent flow has more of an influence on the contraction rate and, depending upon the direction of the relative flow,

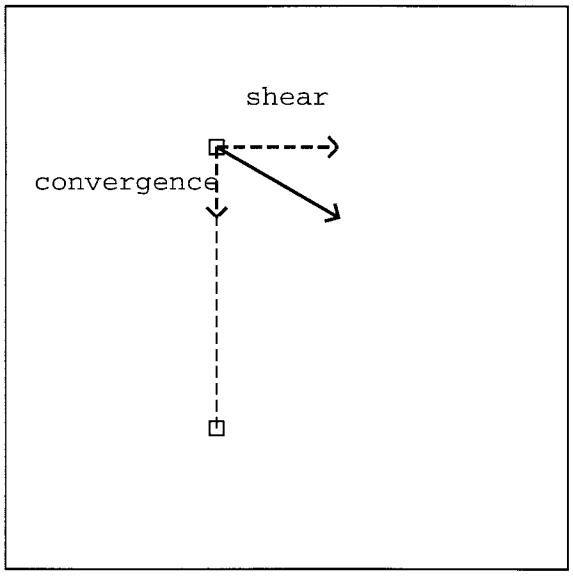

FIG. 5. The relative flow of one parcel relative to another, separated into converging and shearing portions.

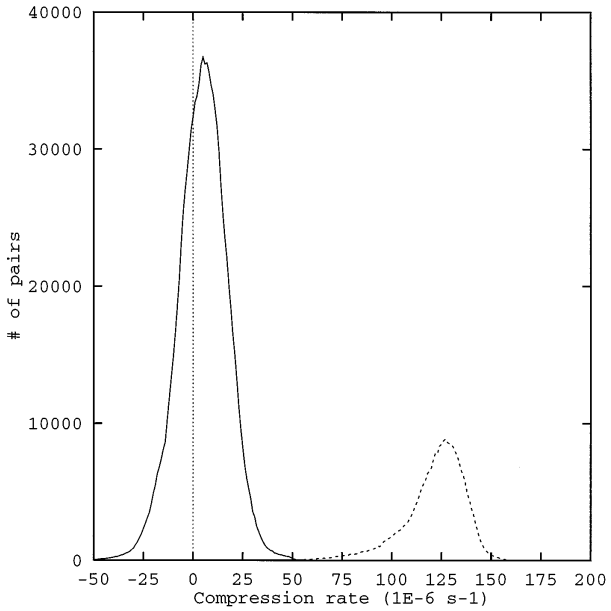

FIG. 6. The distribution of contraction rates (10^{-6} s^{-1}) experienced by a survey of parcel pairs for 12 h ending at 0300 UTC 4 January 1989, as evidenced by a numerical simulation initialized at 1200 UTC 3 January. Contraction rates are obtained using a $99 \times 59 \times 49$ grid with 0.3° spacing in the horizontal and 0.2-km (σ_z) spacing in the vertical (from 0.2 to 9.8 km). The solid and dashed lines represent the C distribution for those pairs lying in the horizontal and vertical planes, respectively (see Fig. 1). Contraction rates were calculated via Eq. (2).

the parcels may separate or compress. Since steady-state convergence or divergence is physically impossible in the nearly incompressible flow of the atmosphere, over long periods it is expected that the pair will experience both convergence and divergence. This implies that the long-term contraction rate is not greatly influenced by the convergent flow.

At longer timescales, the shearing flow has more of an influence. This is because the effect is the same regardless of the direction of the relative flow. The shearing flow is always associated with the separation of parcels in the future and contraction of parcels during the past. As a result, the long-term contraction rate is dominated by the shear rather than convergence. Such a conclusion is supported by studies on chaotic advection (Aref 1984).

Since separation in the past is represented by positive contraction rates, the distribution of contraction rates should be shifted toward positive values. Such a shift is found in the model output. However, the amount of shift depends upon the initial orientation of the parcel pair. To illustrate, the 12-h contraction rates valid at 0300 UTC 4 January 1989 were calculated for all horizontally or vertically oriented pairs of adjacent grid points on the trajectory grid. The solid line in Fig. 6 represents the C distribution computed from horizontally oriented pairs, while the dashed line represents the C distribution computed from vertically oriented pairs.

The contraction rates associated with vertically oriented pairs are much greater than those associated with horizontally oriented pairs. This means that parcel histories are much more sensitive to vertical (as opposed to horizontal) differences in position. Evidently, there is a greater variation in the three-dimensional wind along the vertical axis than along the horizontal plane; that is, the vertical shear tends to be large relative to the horizontal shear.

b. Vertical scale factor

Unless vertical distances are multipled by a scaling factor, the signal contained in the horizontal dependency will be overwhelmed by that contained in the vertical dependency. Since the shift in Fig. 6 is due to the difference in scale between the vertical and horizontal shear, the scaling factor is set as the ratio of the average vertical shear to the average horizontal shear, as simulated by the model; that is,

$$s = \left(\overline{\frac{dv}{dz}}\right)\left(\overline{\frac{dv}{dx}}\right)^{-1},$$

where s is the scaling factor. Since the shear of the vertical velocity is about two orders of magnitude smaller than the shear of the horizontal velocity, only the horizontal velocity is used in the calculation. In addition, to simplify the calculations, the shear of the u component is determined separately from the shear of the v component. The scaling factor is taken as the average of the components.

The scaling factor, as calculated in this way, is not a constant. A large scaling factor is expected during times

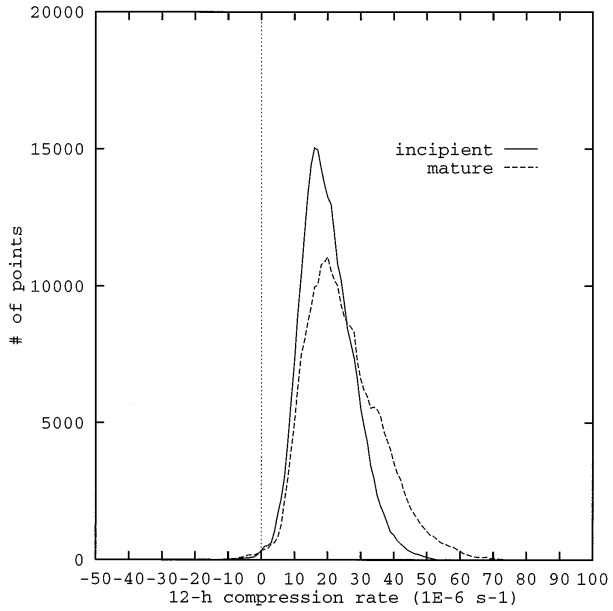

FIG. 7. Distribution of contraction rates (10^{-6} s^{-1}) for trajectory grid points at 0300 UTC (solid line) and 1800 UTC (dashed line) 4 January 1989, as evidenced by a numerical simulation initialized at 1200 UTC 3 January. Contraction rates were calculated as discussed in the text. Vertical distances were scaled by 150.

when the horizontal shear is weak and/or the vertical shear is strong. Conversely, a small scaling factor is expected during times when the horizontal wind shear is strong and/or when the vertical wind shear is weak. Strong/weak horizontal shear can happen when the horizontal winds are strong/weak. Strong vertical shear can happen in strongly baroclinic flows and when the flow is vertically stratified such that the vertical mixing is small. Weak vertical shear can happen when the flow is well mixed.

Such variation is illustrated by calculations of s at various times in the simulation of the ERICA IOP 4 storm. For the incipient stage of the storm (0300 UTC 4 January 1989), s is found to be 160 (using the entire model domain). For the mature stage of the storm (1800 UTC 4 January 1989), s is found to be 148. Using a selected subdomain in which the cyclone is located (the trajectory grid domain shown in Fig. 3), s is found to be smaller—that is, 115 and 90 for the incipient and mature stages, respectively.

Although the vertical scale factor is not constant, it may be desirable to use the same value to allow quantitative comparisons of contraction rates. For the purposes of this paper, a scale factor of 150 is used. The contraction distribution with $s = 150$ is shown in Fig. 7. For comparison, the typical Lyapunov exponent for two-dimensional atmospheric flows as determined by Pierrehumbert and Yang (1993) is on the order of 0.3 day^{-1} or 5×10^{-6} s^{-1} (see their Fig. 10).

One must also recognize that, since s magnifies vertical differences, raising s lowers contraction rates for pairs oriented along the vertical axis at time 0 [via increased $r(0)$], thereby minimizing the identification of horizontally oriented boundaries (i.e., boundaries between pairs oriented along the vertical axis). At the same time, raising s also accentuates differences in the integrated vertical motion [by increasing the vertical component of $r(t)$], thereby maximizing the identification of boundaries between ascending and descending airstreams. One's choice of s is thus constrained by the type of details to be identified as well as the state of the atmosphere.

c. Threshold selection

At 0300 UTC 4 January 1989, the storm of interest (ERICA IOP 4) is in its incipient stage and the contraction distribution shows a lack of strong contraction rates (solid line in Fig. 7) in comparison to the mature stage (dashed line). Since airstream boundaries are associated with high contraction rates (see section 2c), the higher contraction rates of the mature stage can be attributed to the presence of strong airstream boundaries at that time (see, e.g., Cohen 1993). In this sense, Fig. 7 hints that C values greater than 40×10^{-6} s^{-1} are representative of these more intense boudaries and, as such, can be used as a criterion for their identification. As such, 40×10^{-6} s^{-1} can be used as a threshold. Areas with contraction rates above this threshold will correspond to intense airstream boundaries.

While one's threshold will depend upon the specific domain, case, and time (e.g., one should use a threshold less than 40×10^{-6} s^{-1} to identify the dominant airstream boundaries during the incipient stage of the ERICA IOP 4 storm), it may be desirable to use the same threshold for comparison purposes. A review of other C distributions (not shown) shows that a value of 40×10^{-6} s^{-1} as a threshold is appropriate in the identification of strong airstream boundaries such as those present in the case studied here.

d. Timescale

The contraction values shown in Figs. 6 and 7 are obtained by using (2) with $|t| = 12$ h (see section 3). By using a lifetime of 12 h, only those regions that experience conditions favorable for the development of airstream boundaries over 12 h will contribute to the high end of the C values.

One can vary t to identify airstream boundaries that develop over different lengths of time. However, the variance in the C distribution is different, and consequently a different C threshold is needed to clearly identify the intense airstream boundaries. Figure 8 shows the distribution of C values obtained when a timescale of 6 h, rather than 12 h, is used. Comparing Figs. 7 and 8 reveals that shortening $|t|$ leads to a greater spread in C values. Conversely, as $|t|$ increases, the C distribution narrows (e.g., see Fig. 10 of Pierrehumbert and Yang

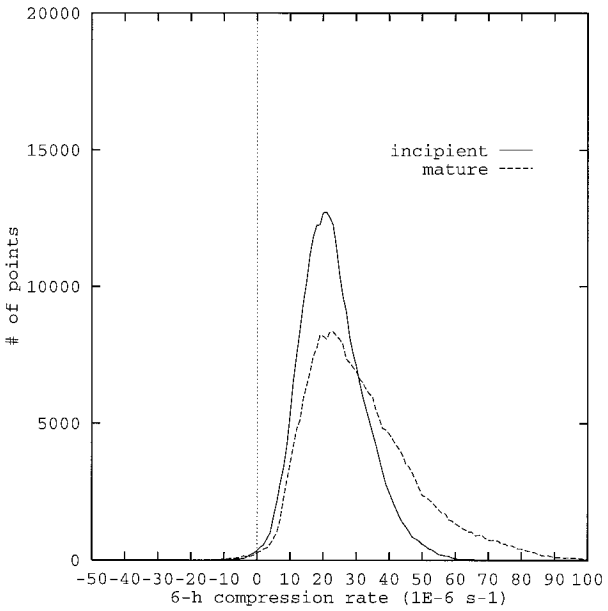

FIG. 8. Distribution of contraction rates (10^{-6} s^{-1}) as in Fig. 7 except that trajectory lifetimes were 6 h rather than 12 h.

1993). The placement of the peak value is about the same in Figs. 7 and 8 (i.e., $C_{\text{mode}} \sim 20 \times 10^{-6}$ s^{-1}), although the C values for the incipient stage and longer lifetimes tend to be lower than values for the mature stage and shorter lifetimes. The variation with cyclone development is consistent with the discussion in the previous section. The variation with lifetime is also expected since the atmosphere has a limited domain—that is, r is limited while $|t|$ continues to grow. As such, all C values should approach zero as $|t|$ approaches infinity.

An appropriate C threshold can be estimated for $|t|$ other than 12 h by assuming that the width of the C distribution decreases as $|t|^{-1/2}$ (as in a binomial distribution):

$$C_0(t) - C_{\text{mode}} \propto |t|^{-1/2},$$

where $(C_0 - C_{\text{mode}})$ is used as a measure of the spread. Using $C_0(-12 \text{ h}) = 40 \times 10^{-6}$ s^{-1} and $C_{\text{mode}} = 20 \times 10^{-6}$ s^{-1}, one obtains

$$[C_0(t) - C_{\text{mode}}]|t|^{1/2} = (20 \times 10^{-6}\text{s}^{-1})(12 \text{ h})^{1/2}$$

$$[C_0(t) - C_{\text{mode}}]^2|t| \sim 17 \times 10^{-6} \text{ s}^{-1}. \quad (3)$$

This suggests that $C_0(-6 \text{ h}) \sim 48 \times 10^{-6}$ s^{-1}. While such a value appears consistent with Fig. 8, additional trials are needed at various $|t|$ to more fully ascertain the validity of (3).

5. Graphing

In this and following sections, the second simulation of ERICA IOP 4 is used. The rationale for the different simulations is given in section 3.

Once the values of C are obtained by (2) for each grid point (using the parameters and procedure outlined in section 3), the contraction rate can be plotted (see Fig. 9). To emphasize the contraction rate gradient, the shading increments are

$$C_i = C_0(i^{0.25}),$$

where C_0 is 40×10^{-6} s^{-1} and C_i is the minimum contraction rate corresponding to the ith shade.

As is evident in Fig. 9, the high contraction rates are associated with zones that are oriented linearly and, for the most part, are coincident with the gradients in potential temperature and/or troughs in pressure. Analysis of the storm at different heights and times indicates that such a structure is temporally and spatially continuous (see Cohen 1993).

6. Sensitivity tests

a. Sensitivity to trajectory grid

The effects of the trajectory grid position and spacing on the analysis of the airstream boundaries are ascertained by visually comparing different runs. Varying the trajectory grid position has virtually no effect on the results (not shown). This is encouraging because it implies that the technique is quite stable.

To evaluate the effect of the grid spacing, a new trajectory grid was constructed at twice the resolution but over a limited domain (see box in Fig. 9) The analysis for this smaller domain is shown in Fig. 10 based upon the original trajectory grid and in Fig. 11 based upon the higher resolution trajectory grid. These figures show that the trajectory grid spacing affects the detail within, but not the placement of, the analyzed airstream boundaries.

b. Sensitivity to trajectory parameters

To assess the sensitivity of the identification technique to parameters in the trajectory calculation procedure, the parameters are varied and the resulting analyses are compared. The three parameters are the number of wind correction steps, the wind data step, and the integration step. The best product should be obtained by using the most wind correction steps and the smallest wind data and integration steps. Figure 12 shows the result obtained when six correction steps are made using wind data every 15 min and an integration step of 5 min (hereafter the control case). Visually comparing this figure against Fig. 9 reveals that very little information is lost by using only two correction steps with wind data every 60 min and an integration step of 15 min.

To quantify the effect of changing the calculation parameters, each parameter was varied. The resulting contraction rates (hereafter the test cases) were compared grid point by grid point with the control case. Figure 13 shows the number of grid points that meet

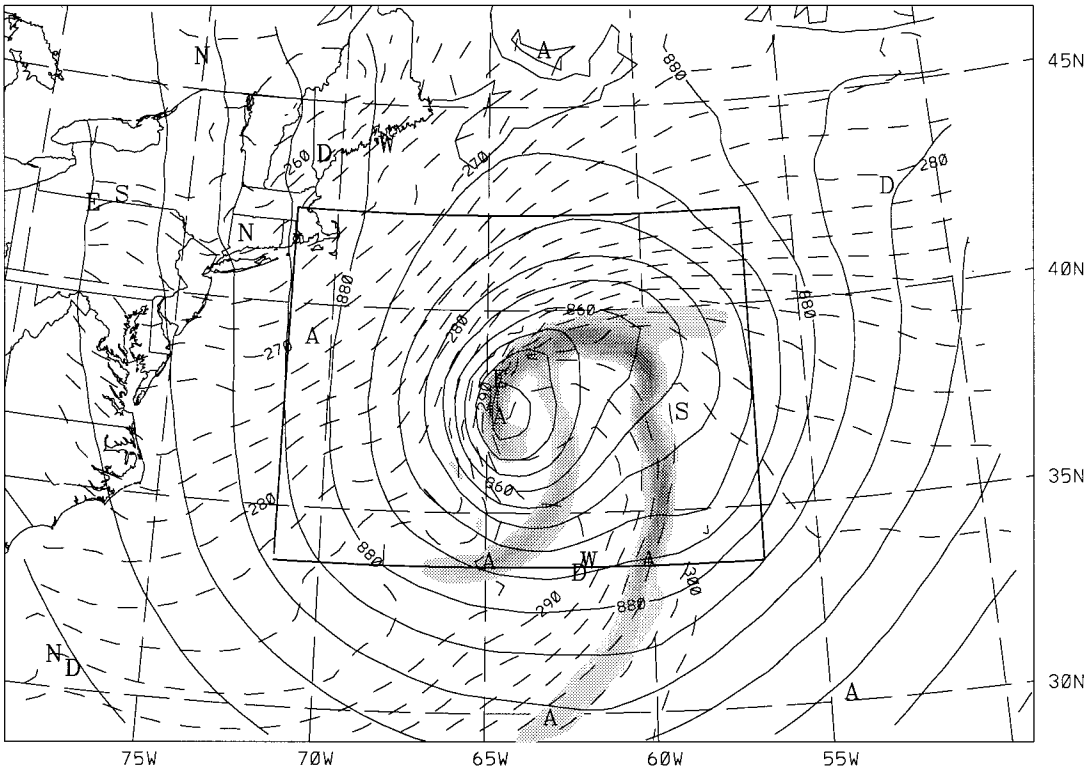

FIG. 9. Pressure (mb, solid lines), virtual potential temperature (K, dashed lines), and airstream boundaries (shading) at $z = 1$ km for the simulation of ERICA IOP 4 on 1800 UTC 4 January 1989 (initialized at 0000 UTC 4 January 1989). Points of maximum and minimum longitudinal, latitudinal, and vertical displacement are identified by letters (N, S, E, W, A, and D). Boxed area corresponds to horizontal domain shown in Figs. 10 and 11.

the contraction rate threshold in the control case but fail to meet it in the test case or vice versa, relative to the number that meet it in the control case (in percent). This percentage (hereafter the placement error) will thus be 100% if the analyzed airstream boundaries disappear entirely and 200% if the boundaries have the same structure but are shifted into an entirely different region.

The greatest effect on the placement error is produced by changing the wind data step (see solid line in Fig. 13). The error essentially increases linearly at about 3.7% $(15\ \text{min})^{-1}$. Using a 180-min wind data step has an error of about 40% (not shown). Since the airstream configuration is similar (e.g., cf. Figs. 9 and 12), the error is apparently due to the placement of the airstream boundaries. With this in mind, it appears acceptable to use a 60-min data step to diagnose the synoptic-scale airstream configuration, especially near the surface.

The dashed line in Fig. 13 is obtained by varying the number of wind corrections. Since these runs are obtained using a 60-min data step, the error relative to that obtained with a 15 min data step hovers around 10%. This shows that the number of wind corrections has little effect on the analysis as long as more than one wind correction step is used.

The dotted line is obtained by varying the integration step. Like the tests made on the wind corrections, these runs are obtained using a 60-min data step, causing the error relative to that obtained with a 15 min data step to be around 10%. The analysis shows little change when the integration time step is changed from 5 to 20 min. Thus, there appears to be little advantage to using more than three integration steps per wind data step.

In a quantitative treatment of trajectory errors, Seibert (1993) suggested that a wind data step of 30 min and an integration step of $0.5\ \Delta x/u \approx 12$ min be used but cautioned that position errors can amplify in deformation flow. Since airstream boundaries form in deformation flow, one might expect a study of the airstream boundaries to meet stricter standards. However, the sensitivity studies performed show that this technique is highly robust. By utilizing ensembles of trajectories, the technique is less sensitive than studies have suggested for individual trajectories.

7. Applications

It is suspected that there are a host of situations to which this technique can be applied. A sampling is given here of possible areas of application.

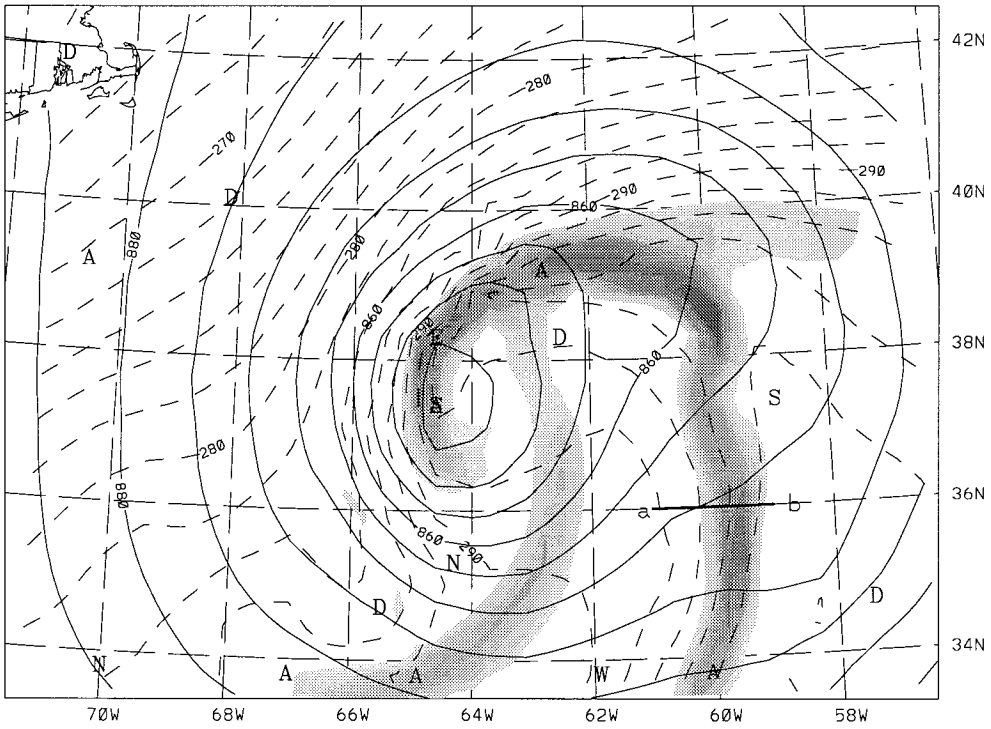

FIG. 10. Same as Fig. 9 except for a smaller horizontal domain (indicated by boxed area shown in Fig. 9). Line *ab* indicates the position of the cross section shown in Fig. 19.

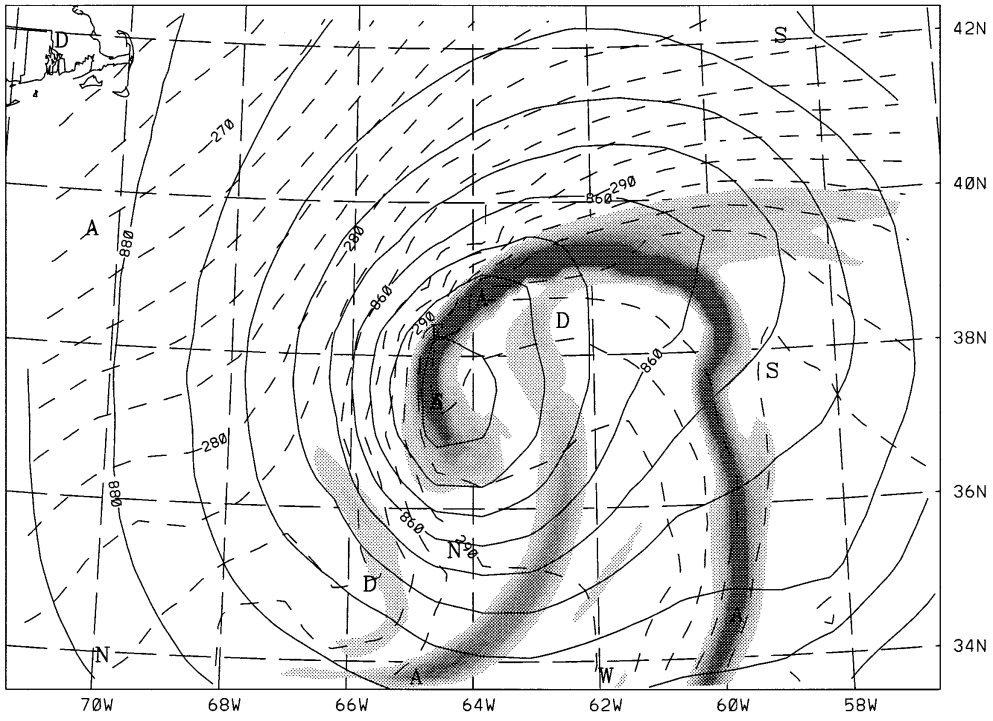

FIG. 11. Same as Fig. 10 except the trajectory grid spacing was 0.15° rather than 0.3°.

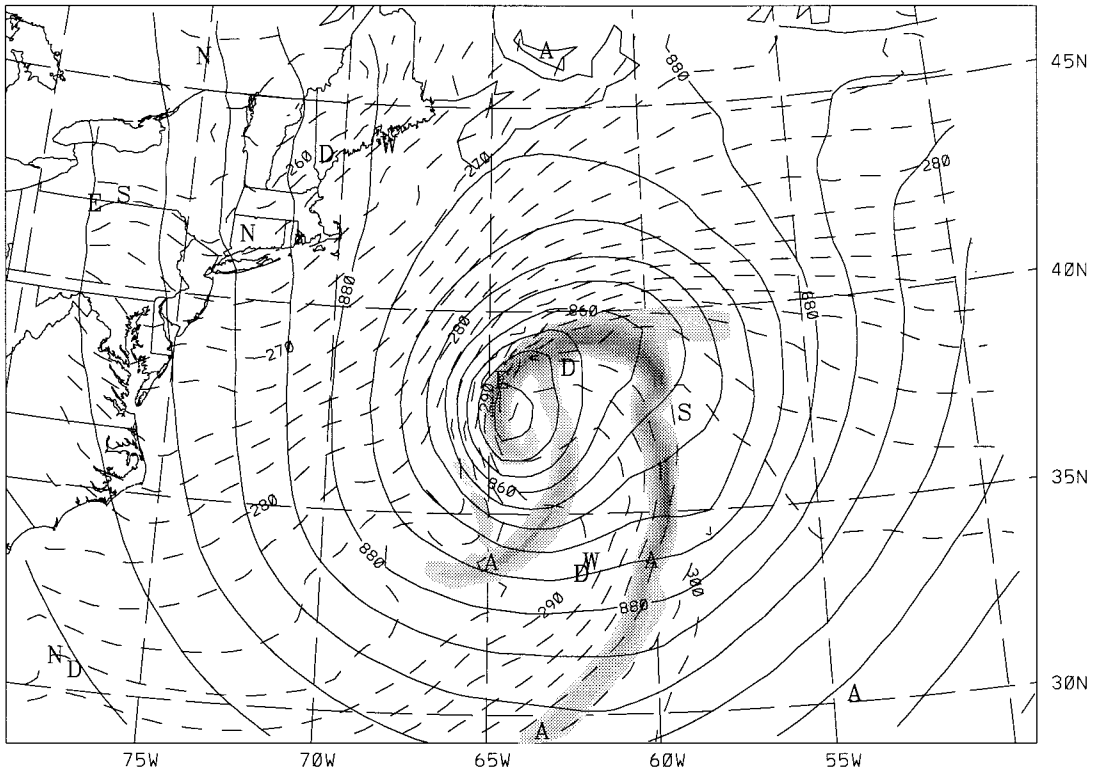

FIG. 12. Same as Fig. 9 except that trajectories were calculated using six correction steps and winds every 15 min integrated with 5-min steps.

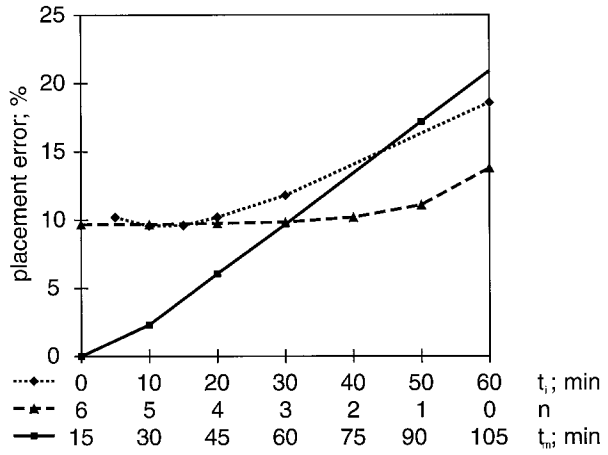

FIG. 13. Placement error (percentage of grid points that meet the contraction rate threshold in the control case but fail to meet it in the test case or vice versa; in percentage of grid points that meet it in the control case) associated with changes in trajectory calculation: wind data step t_m (min, solid line with boxes), number of wind corrections (n, dashed line with triangles), and wind integration step t_i (min, dotted line with diamonds). When t_m is varied, $n = 6$ and $t_i = 5$ min. When n is varied, $t_w = 60$ min and $t_i = 5$ min. When t_i is varied, $t_w = 60$ min and $n = 2$. In each case, the result is compared with the one obtained using t_w, n, and t_i equal to 15 min, 6, and 5 min, respectively.

a. Identification of airstreams and their boundaries

The most obvious application, perhaps, is the identification of airstream boundaries. Not only is the procedure well defined, but the technique allows one to identify the airstream boundaries with much more precision than has typically been done in the past. This is because the speed of the computer facilitates the analysis of a large number of trajectories. As a result, a relatively dense grid of trajectories can be used to produce highly defined airstream boundaries.

For example, consider the situation shown in Fig. 14. By plotting the trajectories (at half the resolution of the model grid), one can get a sense of the presence of some boundaries but it is difficult to determine a position with much precision, particularly in the region of the seclusion and occlusion. When one uses the technique described above, the position of the boundaries becomes clear (see Fig. 9) since the dense grid of trajectories allows a relatively precise placement of the boundaries. A manual analysis of such a large number of trajectories would be daunting.

The identification of the airstream boundaries also provides a general picture of the airstreams. From Fig. 9, one can see the letters A, D, W, E, N, and S at various places. These are objectively plotted by the computer along with the airstream boundaries. By identifying the regions of relative maxima and minima of 12-h inte-

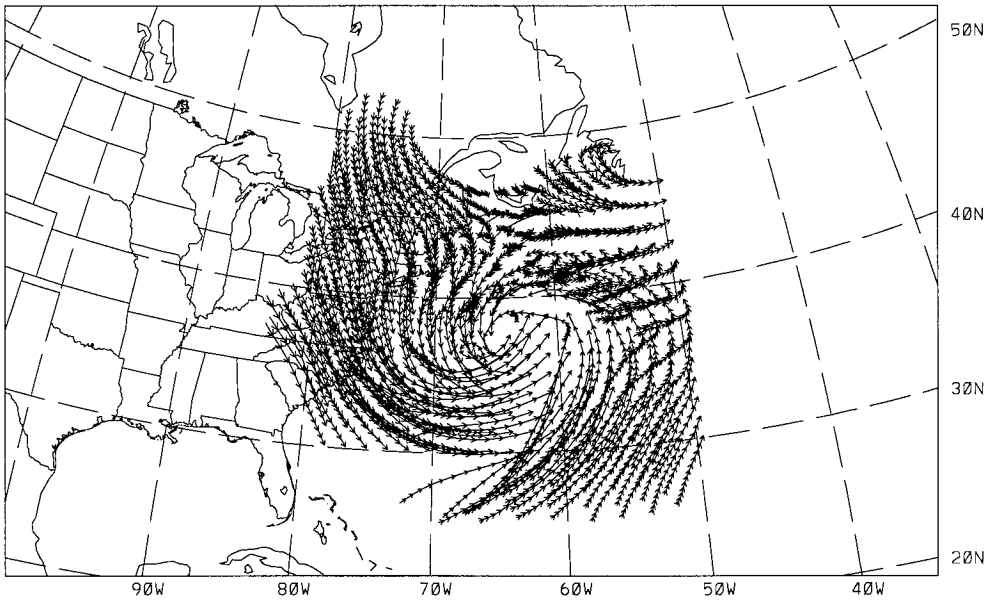

FIG. 14. A grid of 12-h backward trajectories, calculated as in the text and colocated with the trajectory grid but at half the resolution of the model grid, ending at a height of 1 km at 1800 UTC 4 January 1989. Each hour of a trajectory's history is marked by an arrow. The size of the arrow is proportional to the trajectory's height.

grated vertical (A and D), latitudinal (N and S), and longitudinal (W and E) motion, the letters can be used to identify the relative source region of the airstream in which the letter is found.

Using this information, one can see that the airstream boundaries separate three distinct regions, each with a distinct source region. A small tongue of descent from the west wraps its way toward the low pressure center. The airstream to the east is characterized by flow from the south. The airstream to the north and west is characterized by relatively weaker displacements (an E is largely hidden by a boundary near the center of circulation). Maxima of ascent are colocated with the airstream boundaries themselves. Such an analysis would normally take several minutes or more, even for one experienced in trajectory analysis, as one would need to view the trajectories individually in order to mentally visualize the structure (D. Schultz 1994, personal communication).

This three-airstream configuration is reminiscent of the three-airstream models (e.g., dry, descending airstream and cold and warm conveyor belts) used in cloud interpretation studies (see, e.g., Browning 1990). The fact that such a configuration is structurally continuous throughout the troposphere and temporally continuous throughout the development of the storm is used as a basis for the structural analysis of occluded cyclones performed by Cohen (1993).

b. Trajectory errors

Since both the uncertainty in the trajectory path and the placement of the airstream boundary can be ascertained by the contraction rate (see section 2c), the uncertainty can be directly related to its placement relative to the airstream boundaries. Consequently, the validity of using an individual trajectory to assess the characteristic history of an airstream can be clearly addressed.

To illustrate, consider the analysis shown in Fig. 15. A warm sector ($\theta_v > 296$ K) southeast of the low center is bounded by a relatively strong temperature gradient to the north and west. The gradients imply the existence of warm and cold fronts, respectively. A common exercise is to calculate trajectories for various points in the region so that the Lagrangian forcing can be diagnosed. Four such trajectories, ending at various points within the colder air, are included in Fig. 15.

As pointed out by Kahl (1993), single trajectories are potentially unrepresentative of the actual airflow, particularly when large wind shear is present. Unfortunately, without any additional information, it is difficult to ascertain the quality of each trajectory calculation. As a result, one cannot say whether the diagnostics based upon the trajectory calculations are valid.

By virtue of their definition, the airstream boundaries provide this information. In Fig. 16, the four trajectories are plotted along with the airstream boundaries. From their placement relative to the airstream boundaries, one can see that trajectory c can be treated with a much higher degree of certainty than the others. The superposition of an airstream boundary upon the final positions of trajectories b and d indicates that the histories of these trajectories are highly dependent upon their final position. Without the airstream boundaries as a guide, one would have to examine an ensemble of tra-

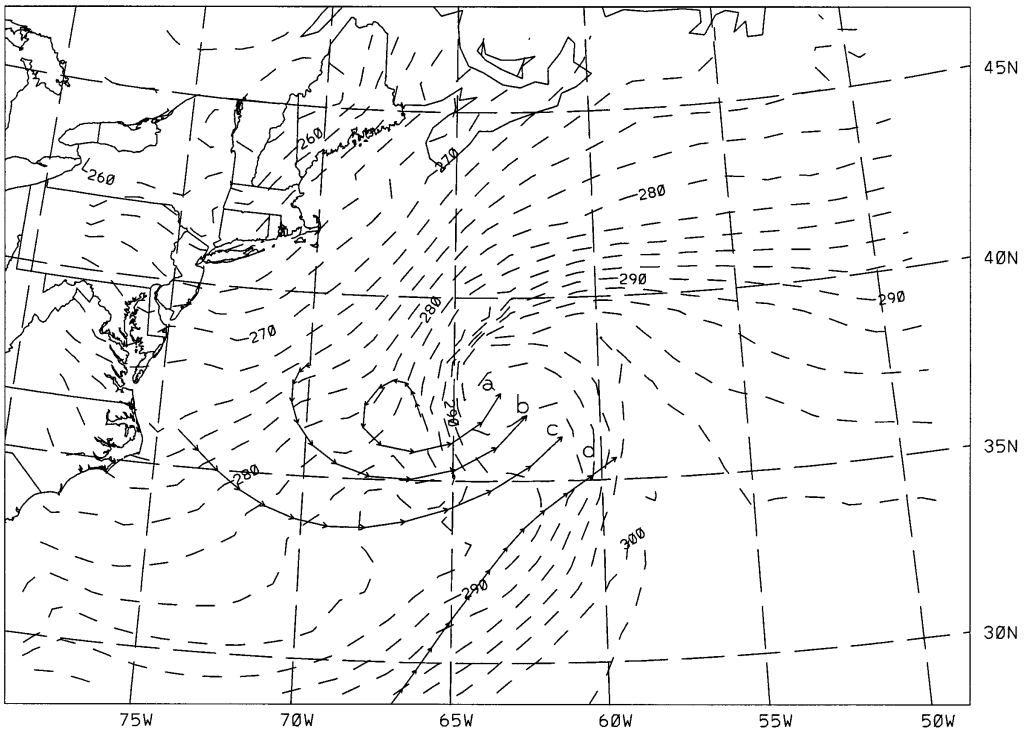

FIG. 15. Same as Fig. 9 except that isobars and airstream boundaries have been removed. Four 12-h trajectories, ending at a height of 1 km at 1800 UTC 4 January 1989, are plotted.

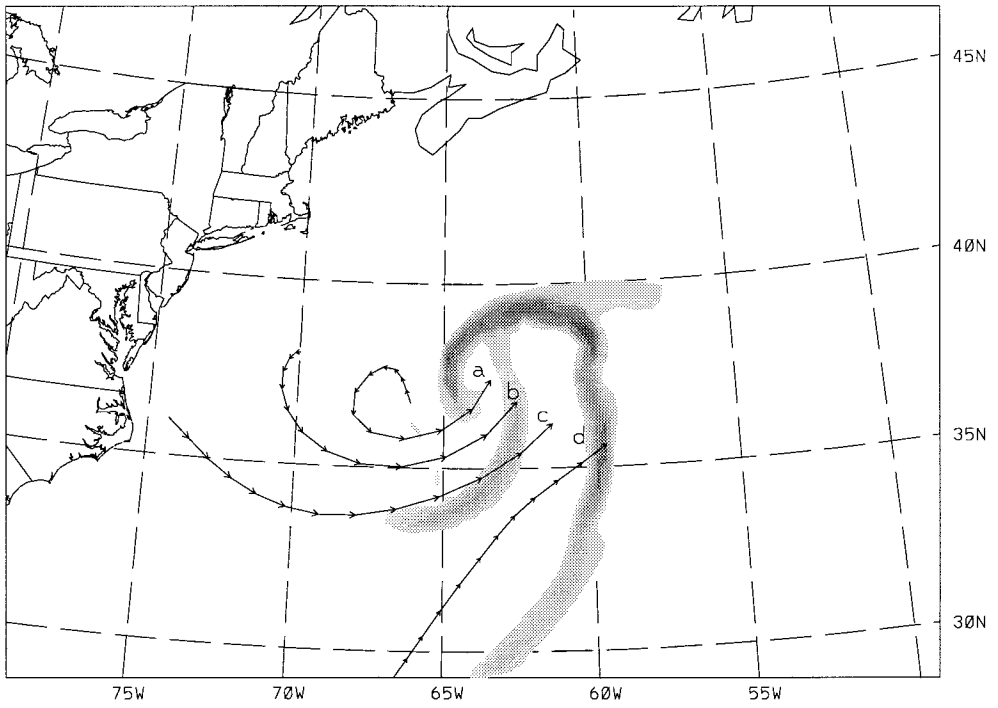

FIG. 16. Same as Fig. 15 except that airstream boundaries are plotted instead of virtual potential temperature.

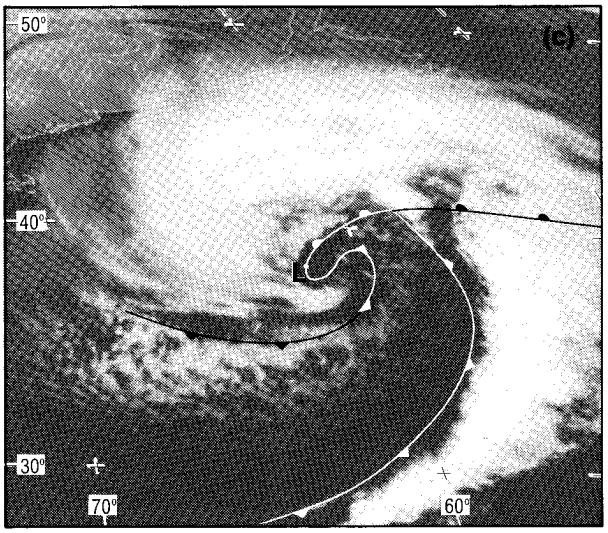

FIG. 17. NOAA GOES-East infrared satellite image at 1800 UTC 4 January 1989 with surface frontal positions. From Fig. 15c of Neiman and Shapiro (1993).

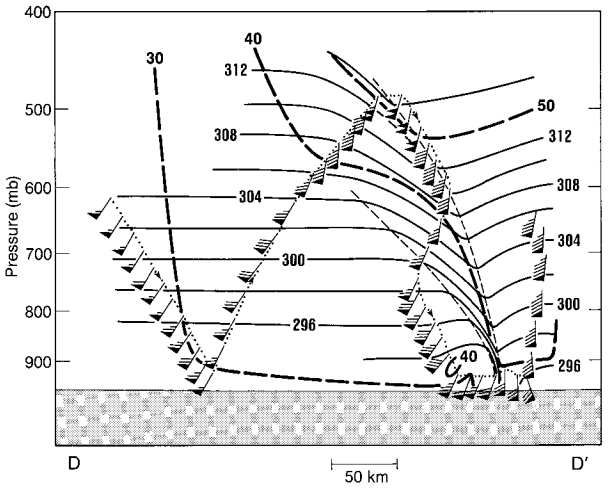

FIG. 18. Cross section of potential temperature (K, solid) and section-normal wind speed (m s^{-1}, bold dashed) along line *DD′* of Fig. 13 of Neiman et al. (1993) on 4 January 1989. Thin-dashed lines are frontal boundaries. NOAA WP-3D flight tracks are depicted by small-dotted lines, with selected flight-level wind vectors plotted. Wind flags and barbs are selected time-to-space-adjusted 350-m flight-level observations. From Fig. 15 of Neiman et al. (1993).

jectories that end at points very close to the final position of each trajectory in question (as in Merrill et al. 1985) or examine the effect of random errors to each wind step, both being techniques recommended by Stohl et al. (1995).

c. Frontal analysis

At first glance, one may be tempted to view the leading edges of airstreams in much the same way as fronts. As mentioned previously, such usage is not recommended. The airstream boundary results from spatial differences in the time-integrated atmospheric forcing. A recognizable signature in an instantaneous field need not be present. A distinction must therefore be made between airstream boundaries and fronts. At the same time, however, it is important to relate the airstream boundaries to the fronts in order to provide a link between the structure of the storm represented by the fronts and that represented by the airstream boundaries.

To illustrate the use of this technique in frontal analysis, two situations are presented. In one case, the airstream boundary is coincident with the front. In the other case, the airstream boundary is not coincident with the front.

The model simulation of the ERICA IOP 4 storm, when initialized at 0000 UTC 4 January 1989, did rather well in reproducing the structure of the storm. Figure 17 shows the frontal analysis based upon the observations valid at the same time (Neiman and Shapiro 1993). The fronts correspond to the observed θ_e gradients (see Fig. 13 of Neiman et al. 1993). The analyzed airstream boundaries, valid at the same time, are found to have the same orientation as the observed fronts (cf. with Fig. 9; position and orientation of airstream boundaries at 300 m are similar to those shown at 1 km).

Not in all situations, however, does the model produce an airstream structure that corresponds to the frontal analysis. Consider the cross section shown in Fig. 18. Here, Neiman et al. analyze a cold front sloping over the cold air along the region of increased baroclinity. The model analysis, shown in Fig. 19, not only fails to capture such baroclinity but also fails to capture any significant airstream boundary sloping over the cold air. On the contrary, leaved airstream boundaries are analyzed sloping over the warm air.

In this case, the model has correctly identified the airstream boundary but failed to identify the baroclinic feature. This is understandable. After all, the thermodynamic feature has too fine a scale to be ''seen'' on the coarse model grid. The analyst, on the other hand, has identified the baroclinic feature but not the airstream boundary. This is because the airstream boundary has no corresponding baroclinic signature; that is, the boundary is not collocated with a front in the traditional sense (except near the surface). While it is unknown to what extent the difference is due to the coarseness of the model grid, it is still important to make the distinction between fronts and airstream boundaries, as stated previously.

8. Summary

Airstream boundaries have been quantitatively investigated in order to provide a framework for their analysis in numerical weather simulations. A summary of the investigation follows.

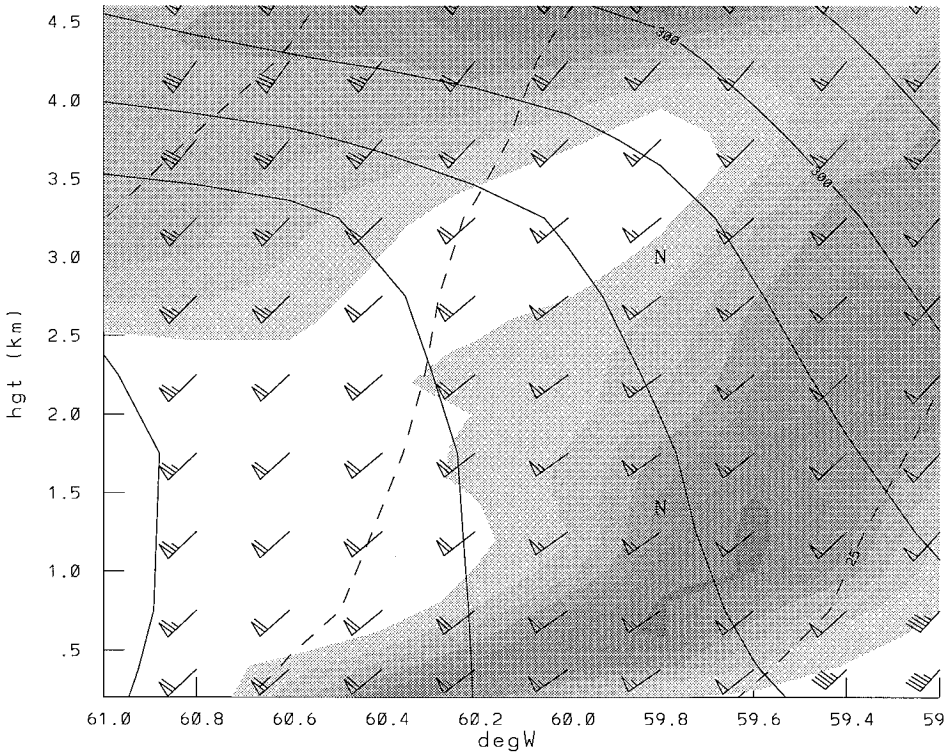

FIG. 19. Virtual potential temperature (K, solid lines), wind speed (m s^{-1}, dashed lines), wind barbs, and airstream boundaries (shading) along line *ab* of Fig. 10 for the simulation of ERICA IOP 4 at 1800 UTC 4 January 1989.

- An airstream has been defined as a region of air in which the spatial history of each portion is similar.
- An airstream boundary has been defined as the surface separating two relatively distinct airstreams.
- The strength of an airstream boundary has been defined in terms of the contraction rate experienced by parcels ending at the location of the boundary.
- The contraction rate has been defined in (2).
- The vertical to horizontal scale of atmospheric flow is evidenced by different contraction rates along the vertical versus the horizontal. This scale will vary but was found to be about 1:150 by comparing the average horizontal shear with the average vertical shear, as simulated by the numerical model, within the model domain.
- Intense 12-h airstream boundaries, such as those present in the mature phase of ERICA IOP 4, are associated with contraction rates greater than 40×10^{-6} s^{-1} [~ 1 $(6\ h)^{-1}$].
- Intense airstream boundaries at other trajectory lifetimes can be identified using the threshold given by (3).

Having quantified airstream boundaries in this way, the boundaries can be identified (within numerical simulations) by using a high density of backward trajectories over the domain of interest. Since this technique uses groups of trajectories, it is not unduly sensitive to the spatial and temporal resolution of the model output and can be performed with modest computational burden. A summary of the sensitivity study follows.

- The identification of airstream boundaries is not sensitive to trajectory grid placement.
- Neither the number of wind correction steps nor the number of integration steps has a strong effect on the identification scheme as long as at least two wind corrections are made and three integration steps are used (i.e., 20 min for a 60-min wind data step).
- The highest area of sensitivity lies in the dependence upon the wind data step used, with about a 3.7% increase in placement error of intense airstream boundaries for each 15-min increase in wind data step.

Armed with a quick and straightforward method of identifying airstream boundaries, a host of situations can be attacked without having to defend an analysis obtained through more subjective means. Applications include the identification of the airstreams themselves, an estimate of individual trajectory errors, and the analysis of frontal structures.

Acknowledgments. The authors thank the anonymous reviewers for their helpful comments. This research has been supported by the Marine Meteorology Program,

Office of Naval Research Grant N00014-92-J-1577, and the Mesoscale Dynamics Program, Atmospheric Science Division, National Science Foundation Grant ATM-9112508.

REFERENCES

Aref, H., 1984: Stirring by chaotic advection. *J. Fluid. Mech.*, **143,** 1–21.

Bjerknes, J., and H. Solberg, 1922: Life cycle of cyclones and the polar front theory of atmospheric circulation. *Geof. Publ.*, **3,** 1–18.

Browning, K. A., 1971: Radar measurements of air motion near fronts. *Weather,* **26,** 320–340.

——, 1990: Organization of clouds and precipitation in extratropical cyclones. *Extratropical Cyclones: The Erik Palmén Memorial Volume,* C. W. Newton and E. O. Holopainen, Eds., Amer. Meteor. Soc., 129–153.

Carlson, T. N., 1980: Airflow through midlatitude cyclones and the comma cloud pattern. *Mon. Wea. Rev.,* **108,** 1498–1509.

Chang, S. W., R. J. Alliss, S. Raman, and J.-J. Shi, 1993: SSM/I observations of ERICA IOP 4 marine cyclone: A comparison with in-situ observations and model simulation. *Mon. Wea. Rev.,* **121,** 2452–2464.

Cohen, R. A., 1993: An air stream analysis of the occluded cyclone. Ph.D. dissertation, Drexel University, 209 pp.

Hadlock, R., and C. W. Kreitzberg, 1988: The Experiment on Rapidly Intensifying Cyclones over the Atlantic (ERICA) field study: Objectives and plans. *Bull. Amer. Meteor. Soc.,* **69,** 1309–1320.

Halley, E., 1686: An historical account of the trade winds and monsoons. *Trans. Roy. Soc. London,* **16,** 153–168.

Hartnett, E., G. Forbes, and R. Hadlock, 1989: ERICA, Experiment on Rapidly Intensifying Cyclones over the Atlantic: Field phase summary. [Available from ERICA Data Center, Dept. of Physics and Atmospheric Sciences, Drexel University, Philadelphia, PA 19104.]

Huschke, R. E., Ed., 1959: *Glossary of Meteorology.* Amer. Meteor. Soc., 638 pp.

Kahl, J. D., 1993: A cautionary note on the use of air trajectories in interpreting atmospheric chemistry measurements. *Atmos. Environ.,* **27A,** 3037–3038.

Kutzbach, G., 1979: *The Thermal Theory of Cyclones: A History of Meteorological Thought in the Nineteenth Century*. Amer. Meteor. Soc., 255 pp.

Lempfert, R. G. K., and R. Corless, 1910: Line-squalls and associated phenomena. *Quart. J. Roy. Meteor. Soc.,* **36,** 135–170.

Ley, C. L., 1877: Relation between upper and under currents of the atmosphere around areas of barometric depression. *Quart. J. Roy. Meteor. Soc.,* **3,** 437–445.

Merrill, J. T., R. Bleck, and L. Avila, 1985: Modeling atmospheric transport to the Marshall Islands. *J. Geophys. Res.,* **90,** 12 927–12 936.

Neiman, P. J., and M. A. Shapiro, 1993: The life cycle of an extratropical marine cyclone. Part I: Frontal-cyclone evolution and thermodynamic air–sea interaction. *Mon. Wea. Rev.,* **121,** 2153–2176.

——,——, and L. S. Fedor, 1993: The life cycle of an extratropical marine cyclone. Part II: Mesoscale structure and diagnostics. *Mon. Wea. Rev.,* **121,** 2177–2199.

Pierrehumbert, R. T., and H. Yang, 1993: Global chaotic mixing on isentropic surfaces. *J. Atmos. Sci.,* **50,** 2462–2480.

Schär, C., and H. Wernli, 1993: Structure and evolution of an isolated semi-geostrophic cyclone. *Quart. J. Roy. Meteor. Soc.,* **119,** 57–90.

Schultz, D. M., and C. F. Mass, 1993: The occlusion process in a midlatitude cyclone over land. *Mon. Wea. Rev.,* **121,** 918–940.

Seibert, P., 1993: Convergence and accuracy of numerical methods for trajectory calculations. *J. Appl. Meteor.,* **32,** 558–566.

Shaw, N., 1928: *Manual of Meteorology*. Vol. 2, *Comparative Meteorology,* Cambridge University Press, 445 pp.

——, and R. G. K. Lempfert, 1905: The life history of surface air currents: A study of the surface trajectories of moving air. M.O. Publication 174, London, 107 pp.

Stohl, A., G. Wotawa, P. Seibert, and H. Kromp–Kolb, 1995: Interpolation errors in wind fields as a function of spatial and temporal resolution and their impact on different types of kinematic trajectories. *J. Appl. Meteor.,* **34,** 2149–2165.

Sutton, R., 1994: Lagrangian flow in the middle atmosphere. *Quart. J. Roy. Meteor. Soc.,* **120,** 1299–1321.

Thompson, B. W., 1951: An essay on the general circulation of the atmosphere over South-east Asia and the west Pacific. *Quart. J. Roy. Meteor. Soc.,* **77,** 569–587.

Uccellini, L. W., 1990: Processes contributing to the rapid development of extratropical cyclones. *Extratropical Cyclones: The Erik Palmén Memorial Volume,* C. W. Newton and E. O. Holopainen, Eds., Amer. Meteor. Soc., 81–105.

Wakimoto, R. M., W. Blier, and C.-W. Liu, 1992: The frontal structure of an explosive oceanic cyclone: Airborne radar observations of ERICA IOP 4. *Mon. Wea. Rev.,* **120,** 1135–1155.

Woolf, H. B., Ed., 1979: *Webster's New Collegiate Dictionary.* Merriam, 1532 pp.